A Hybrid Adaptive Low-Mach-Number/Compressible Method for the Euler Equations

Emmanuel Motheau,* Max Duarte,† Ann Almgren‡ and John B. Bell§

Center for Computational Sciences and Engineering, Lawrence Berkeley National Laboratory,

1 Cyclotron Rd, MS 50A-3111, Berkeley, CA 94720, USA

This paper presents a novel hybrid method for solving the low-Mach-number equations for inviscid flow supplemented with long wavelength acoustics as computed by solving the fully compressible Euler equations. Contrary to previous existing methods, the novelty of the present strategy is that the fully compressible equations are solved without any approximation, and that an adaptive mesh refinement (AMR) framework is employed to optimize the performance of the algorithm. It is demonstrated that compared to a purely compressible approach, the hybrid method allows time-steps of larger magnitude at the finest level, leading to an overall reduction of the computational time.

I. Introduction

Flows in which the primary features of interest do not rely on high-frequency acoustic effects, but in which long-wavelength acoustics play a nontrivial role, present a computational challenge. Integrating the entire domain with low-Mach-number methods[1–8] would remove all acoustic wave propagation, while integrating the entire domain with the fully compressible equations can in some cases be prohibitively expensive due to the CFL time step constraint. For example, simulation of thermoacoustic instabilities[9–14] might require fine resolution of the fluid/chemistry interaction but not require fine resolution of acoustic effects, yet one does not want to neglect the long-wavelength wave propagation and its interaction with the larger domain.

The present paper introduces a new multi-level hybrid algorithm to address these type of phenomena. In this new approach, the fully compressible Euler equations are solved on the entire domain, potentially with local refinement, while their low-Mach-number counterparts are solved on subregions of the domain with higher spatial resolution. The finest of the compressible levels communicates inhomogeneous divergence constraints to the coarsest of the low-Mach-number levels, allowing the low-Mach-number levels to retain the long-wavelength acoustics.

The method is similar to the Multiple Pressure Variables (MPV) first introduced in a set of papers by Munz *et al.*[15–18] The essence of the MPV approach is to decompose the pressure into three terms: the thermodynamic pressure p_0; the acoustic pressure p_1; and the perturbational pressure p_2. The acoustic signal is carried by p_1, and p_2 is used to satisfy the divergence constraint on the low-Mach-number levels and is defined as the solution to a Poisson equation. Different approaches for solving p_1 were proposed in the

*Computational Science PostDoctoral Fellow, Computational Research Division, EMotheau@lbl.gov

†Former Computational Science PostDoctoral Fellow, Computational Research Division, max.duarte@cd-adapco.com

‡Senior Scientist, CCSE Group Lead, Computational Research Division, ASAlmgren@lbl.gov

§Senior Scientist, Chief Scientist, Computational Research Division, JBBell@lbl.gov

aforementioned references, for example by solving a set of Linearized Euler Equations (LEEs) on a grid that is a factor of $1/M$ coarser, where M is a measure of the Mach number of the flow. The novelty of the present paper is that the fully compressible equations are solved without any approximation, and that an adaptive mesh refinement (AMR) framework is employed to optimize the performance of the algorithm. Thus, while the fully compressible equations are solved in the entire domain, with possible additional local refinement, the hybrid strategy developed in the present paper allows refined *patches* where the low-Mach-number equations are solved at finer resolution.

The remainder of this paper is organized as follows. In Section II the hybrid hierarchical grid strategy and governing equations that are solved at each resolution are presented. In Section III the numerical results of a canonical test case are presented to assess the performances of the hybrid method.

II. Hybrid hierarchical grid strategy and governing equations

The key idea of the algorithm developed in the present paper is to separate the acoustic part of the flow from the hydrodynamics, and to retain acoustic effects only at wavelengths at longer length scales than the finest flow features. This is achieved by solving a modified form of the low-Mach-number equations at the resolution required by the fine scale features of the flow, while solving the fully compressible governing equations on a coarser level (or levels) underlying the low-Mach-number levels. Because the compressible equations are not solved at the finest level, the overall time step is reduced by a factor of the ratio of grid resolutions from what it would be in a uniformly fine compressible simulation.

In practice, the grid hierarchy can contain multiple levels for each of the two solution approaches. This fits naturally within the paradigm of block-structured adaptive mesh refiment (AMR), although most published examples of AMR simulations solve the same set of equations at every level. The present algorithm forms the **LAMBDA** code and is developed within the BoxLib package,[19,20] a hybrid C++ /Fortran90 software framework that provides support for the development of parallel structured-grid AMR applications.

The computational domain is discretized into one or more grids on a set of different levels of resolution. The levels are denoted by $l = 1, \cdots, L$. The entire computational domain is covered by the coarsest level ($l = 1$); the finest level is denoted by $l = L$. The finer levels may or may not cover the entire domain; the grids at each level are properly nested in the sense that the union of grids at level $l + 1$ is contained in the union of grids at level l. The fully compressible equations are solved on the *compressible levels*, which are denoted as $l_{\rm Comp} = \{1, \cdots, l_{\rm max\_comp}\}$, while on the *low-Mach levels* denoted as $l_{\rm LM} = \{l_{\rm max\_comp+1}, \cdots, L\}$, the modified low-Mach-number equations are solved. The index max_comp is an integer that denotes here the total number of compressible layers involved in the computation. For ease of implementation of the interpolation procedures, the current algorithm assumes a ratio of 2 in resolution between adjacent levels and that the cell size on each level is independent of direction.

II.A. Governing equations solved on compressible level

The set of fully compressible Euler equations are solved on levels $l_{\mathrm{Comp}} = \{1, \cdots, l_{\mathrm{max\_comp}}\}$. The conservation equations for continuity, momentum and energy are expressed as:

$$\frac{\partial \rho}{\partial t} = -\nabla \cdot (\rho \mathbf{u}) \tag{1}$$

$$\frac{\partial (\rho \mathbf{u})}{\partial t} = -\nabla \cdot (\rho \mathbf{u}\mathbf{u}) - \nabla p_{\mathrm{Comp}} \tag{2}$$

$$\frac{\partial (\rho E)}{\partial t} = -\nabla \cdot (\rho \mathbf{u} E + p_{\mathrm{Comp}} \mathbf{u}) \tag{3}$$

Here, ρ, $\mathbf{u}$ and E are the mass density, the velocity vector and the total energy per unit mass, respectively. The total energy is expressed as $E = e + \mathbf{u} \cdot \mathbf{u}/2$, where e is the specific internal energy. The total pressure p_{Comp} is related to the energy through the following equation of state:

$$p_{\mathrm{Comp}} = (\gamma - 1)\, \rho e \tag{4}$$

where γ is the ratio of the specific heats. Note that Eq. (4) represents a very simplified assumption of the equation of state, and that it will be generalized in future work, for example to deal with reactive Navier-Stokes equations composed of multiple chemical species.

II.B. Governing equations solved on low-Mach levels

The set of governing equations are recast under the low-Mach-number assumption and solved on levels $l_{\mathrm{LM}} = \{l_{\mathrm{max\_comp+1}}, \cdots, L\}$. The conservation equations for continuity, momentum, and energy are, respectively:

$$\frac{\partial \rho}{\partial t} = -\nabla \cdot (\rho \mathbf{u}) \tag{5}$$

$$\frac{\partial \mathbf{u}}{\partial t} = -\mathbf{u} \cdot \nabla \mathbf{u} - \frac{1}{\rho} \nabla (p_0 + p_1 + p_2) \tag{6}$$

$$\frac{\partial (\rho h)}{\partial t} = -\nabla \cdot (\rho \mathbf{u} h) + \frac{\mathrm{D} p_1}{\mathrm{D} t} \tag{7}$$

where $h = e + p/\rho$ is the enthalpy. Eqs. (5)-(7) are accompanied by the following constraint on the velocity:

$$\nabla \cdot \mathbf{u} = \nabla \cdot \mathbf{u}_{\mathrm{Comp}} \tag{8}$$

where $\mathbf{u}_{\mathrm{Comp}}$ is interpolated from the compressible level. As explained in the introduction, the pressure that appears in the low-Mach-number equations is not written as a single term like p_{Comp} in the fully compressible equations, but has been decomposed into three terms: the thermodynamic pressure p_0, the acoustic pressure p_1, and the perturbational pressure p_2. Here, p_0 is constant through the whole simulation, while p_1 is provided from the compressible solution and p_2 is intrinsic to the projection method for the pressure.

II.C. Integration procedure

At the beginning of a time-step, both the compressible and the low-Mach-number equations share the same state variables on all levels. The procedure can be summarized as follows:

1. The time-steps for the fully compressible equations (Δt_{Comp}) as well as the low-Mach-number equations

(Δt_{LM}) have to be computed and synchronized first so as to define a global time-marching procedure.

2. The fully compressible Eqs. (1-3) are advanced in time on the designated compressible levels through the whole time-step, from t^n to t^{n+1}. Note that as $\Delta t_{\mathrm{LM}} \geqslant \Delta t_{\mathrm{Comp}}$, this may involve several sub-steps depending on the flow and mesh configurations. At the end of the procedure, state variables are known on those levels at t^{n+1}.

3. The low-Mach-number Eqs. (5-7) are then advanced in time on the designated low-Mach levels from t^n to t^{n+1}. The terms involving the acoustic pressure p_1 are provided by interpolation from the compressible solution. As the momentum Eq. (6) is advanced through a fractional-step method, a variable-coefficient Poisson equation must be solved to correct the velocity fields. The constraint on the velocity that appears as a source term in the Poisson equation is provided by construction with interpolated values from the compressible solution. At the end of the procedure, state variables on the low-Mach levels are spatially averaged down to the compressible levels and a new time-step can begin.

The present algorithm constitutes the new **LAMBDA** code, and uses routines from the existing codes **CASTRO**[21] and **MAESTRO**.[22] This ease of reuse and demonstrated accuracy of the existing discretizations motivated the choices of the numerical methods employed in the present paper to solve the equations; however, the algorithm presented here could be adapted to use alternate discretizations.

III. Results: 2D mixed waves propagation

The performance of the new hybrid compressible/low-Mach method proposed in the present paper is now assessed with a test case consisting on the propagation and convection of mixed acoustic, entropic and vorticity modes in a 2D square domain.[23] A mean flow is imposed throughout the domain, and an acoustic pulse is placed in the center of the domain, while entropy and vorticity pulses are initialized downstream. These latter pulses are simply convected by the mean flow, while the acoustic pulse generates a circular acoustic wave which radiates throughout the domain in all directions. Furthermore, non-reflecting outflow boundary conditions are imposed in all directions of the domain.

The initial conditions are imposed as follows:

$$\rho^{\mathrm{init}}(x,y) = \rho_{\mathrm{ref}} + \eta_a e^{-\alpha_a\left((x-x_a)^2+(y-y_a)^2\right)} + \eta_e e^{-\alpha_e\left((x-x_e)^2+(y-y_e)^2\right)} \tag{9}$$

$$u^{\mathrm{init}}(x,y) = Mc_{\mathrm{ref}} + (y-y_v)\,\eta_v e^{-\alpha_v\left((x-x_v)^2+(y-y_v)^2\right)} \tag{10}$$

$$v^{\mathrm{init}}(x,y) = -(x-x_v)\,\eta_v e^{-\alpha_v\left((x-x_v)^2+(y-y_v)^2\right)} \tag{11}$$

$$p_0^{\mathrm{init}}(x,y) = \frac{c_{\mathrm{ref}}^2\rho_{\mathrm{ref}}}{\gamma}, \qquad p_1^{\mathrm{init}}(x,y) = c_{\mathrm{ref}}^2\eta_a e^{-\alpha_a\left((x-x_a)^2+(y-y_a)^2\right)} \tag{12}$$

Here the sound speed $c_{\mathrm{ref}} = 200$ m/s and the Mach number $M = 0.2$, with $\gamma = 1.1$ and density $\rho_{\mathrm{ref}} = 1$ kg/m^3. The domain is a square with sides of length $L_x = L_y = 256$ m. In the above expressions, α_x is related to the semi-length of the Gaussian b_x by the relation $\alpha_x = \ln 2/b_x^2$. Finally, the strengths of the pulses are controlled by the following set of parameters:

$$b_a = 15, \quad \eta_a = 0.001, \quad x_a = L_x/2, \quad y_a = L_x/2 \tag{13}$$

$$b_e = 5, \quad \eta_e = 0.0001, \quad x_e = 3L_x/4, \quad y_e = L_x/2 \tag{14}$$

$$b_v = 5, \quad \eta_v = 0.0004, \quad x_v = 3L_x/4, \quad y_v = L_x/2 \tag{15}$$

The test case is computed with 3 different approaches:

- the new hybrid method developed in the present paper,
- by solving only the purely low-Mach-number equations (see Sec. II.B),
- by solving only the purely compressible equations (see Sec. II.A).

Time evolution of the solution is presented in Figure 1. Figure 1(a)-(d) in the top row are the solutions computed with the purely low-Mach-number approach, whereas Figure 1(e)-(h) are solutions computed with the new hybrid method. The compressible solution gives results visually indistinguishable from the hybrid approach so those are not shown here. In both the hybrid and compressible solutions, the circular pressure wave generated from the center of the domain propagates in all directions. As the sound speed is far higher than the mean flow velocity, the acoustic wave passes the entropy pulse and eventually leaves the domain at 0.4 s. When the purely low-Mach-number approach is employed, the pressure pulse in the center of the domain is considered as an entropy pulse, and is convected in the same way as the entropy pulse localized downstream. It is noted that the hybrid solution correctly captures the behavior of the waves generated from acoustic pulse despite the fact that the compressible grid under the acoustic pulse is at lower resolution than in the fully compressible solution, and has an overset fine low Mach number grid.

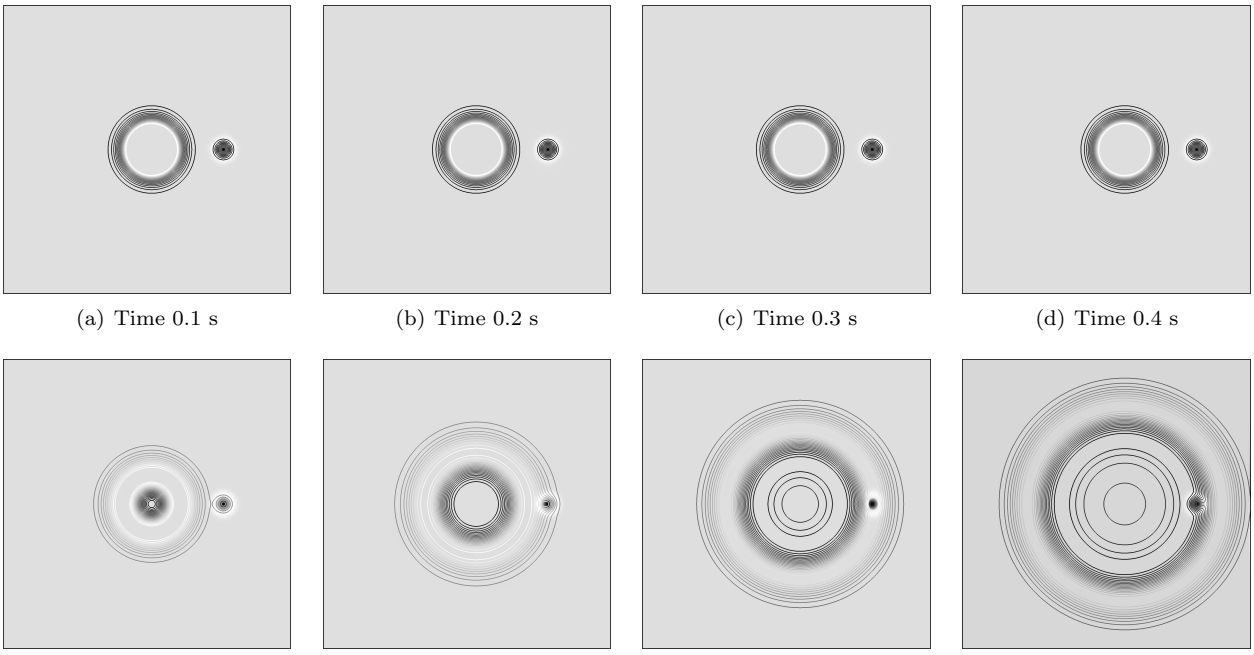

(a) Time 0.1 s (b) Time 0.2 s (c) Time 0.3 s (d) Time 0.4 s

(e) Time 0.1 s (f) Time 0.2 s (g) Time 0.3 s (h) Time 0.4 s

Figure 1. Isocontour of density superimposed on field of vorticity for solutions at $t = 0.1$ s, 0.2 s, 0.3 s and 0.4 s. The top row (figures (a)-(d)) are solutions computed with the purely low-Mach-number approach. The bottom row (figures (e)-(h)) are solutions computed with the hybrid method detailed in the present paper.

In order to provide quantitative results, both the solution computed with the hybrid method and the purely compressible solution are compared to a reference exact analytical solution.[23] The numerical error is assessed by computation of the $\mathcal{L}^2$-norm of the difference between the computed and the reference solutions, which is expressed as follows:

$$\varepsilon_\phi = \mathcal{L}^2_\phi \left(S_{sol} - S_{ref} \right) = \sqrt{\frac{\left(\phi_{sol} - \phi_{ref} \right)^2}{N_x N_y}} \tag{16}$$

where subscripts sol and ref identify the computed and reference solutions, ϕ is the variable investigated, and N_x and N_y are the number of points in the x and y directions. Note that for simplicity, $N_x = N_y$.

Simulations are performed on a multi-levels grid set composed by a total of $L = 5$ levels. The first level $l = 1$ is discretized with $N_x^{l=1} = 32$ and $N_y^{l=1} = 32$ points, while the other levels are progressively discretized with a mesh refinement ratio of a factor of 2. Table. 1 presents the configuration of the multi-levels grid set by providing a summary of N_x and N_y for each level l of mesh refinement.

l	1	2	3	4	5
N_x	32	64	128	256	512
N_y	32	64	128	256	512

Table 1. Summary of the configuration for simulations performed on the 2D mixed modes propagation test case.

Simulations are performed by first selecting, from $l = 1$ to $l = 4$, the level l_{Comp} where the fully compressible Eqs. (1-3) are solved, and then by selecting a successive addition of low-Mach-number levels of mesh refinement, the finest level being designed by L. In total, 10 simulations are performed, and the choices of l_{Comp} and L for each simulation are summarized in Table 2. Furthermore, ε_ϕ is computed for solutions taken at the time $t = 0.3$ s.

l_{Comp} \ L	1	2	3	4	5
1		×	×	×	×
2			×	×	×
3				×	×
4					×

Table 2. Summary of the choices of l_{Comp} and L for all simulations performed during spatial convergence test of the hybrid method with the propagation of mixed acoustic, entropic and vorticity modes in a 2D square domain.

Figures 2.(a) and 2.(b) present the $\mathcal{L}^2$ norm error computed for the density (ε_ρ) and the velocity in the y-direction (ε_v), respectively. Circle, diamond, square and cross symbols represent l_{Comp} set at $l = 1$, $l = 2$, $l = 3$ and $l = 4$, respectively. This corresponds to a discretization of $N_x = 32, 64, 128$ and 256 points, respectively. Moreover, the dashed lines represent ε_ρ and ε_v evaluated from the solutions computed with the purely compressible equations, while the solid line is the second order slope.

Note here that ε_ρ and ε_v are not computed in the full 2D domain but only on the $x-$axis taken at $y = L_x/2$. This specific choice enable us to separate the contribution of acoustic, entropic and vorticity modes. Indeed, as the axis is taken along the propagation of the acoustic wave, no contribution from the acoustic and entropic modes should appear in the v component of the velocity, but only the ones from the vortex structure. In contrary, on this specific axis, only acoustic and entropic modes should contribute to the evaluation of the density, and not the vorticity mode.

In Figure. 2.(a), the evaluation of ε_ρ for the solutions computed with the purely compressible equations (dashed line) follows a second order rate of convergence, and starts to reach a plateau for levels $l > 3$ (viz. $N_x > 128$). When the hybrid method is employed, the contribution of solving the low-Mach-number equations on an additional level significantly reduces ε_ρ to approximately get the same error as if the additional layer was employed to solve the fully compressible equations. However, solving the low-Mach-number equations on additional finest levels does not help significantly to further reduces ε_ρ, which also

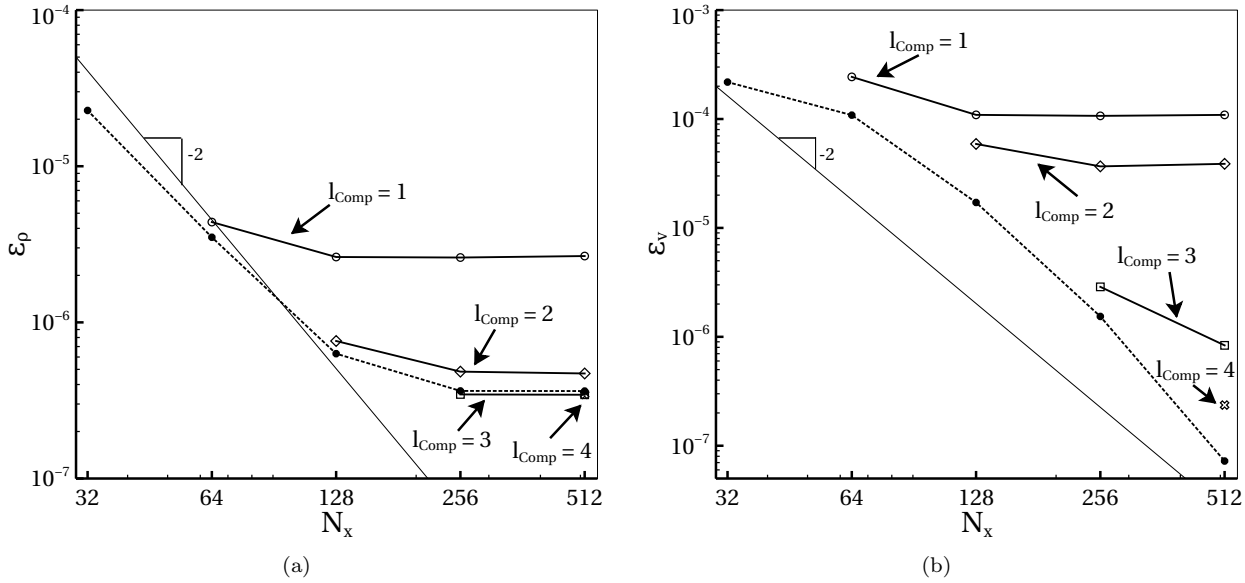

Figure 2. $\mathcal{L}^2$-norm of the discretization error for different maximum level L of mesh refinement for the low-Mach-number equations: (a) ε_ρ for the density, (b) ε_v for the velocity in the y-direction. Circle, diamond, square and cross symbols represent the fully compressible equations solved on the level l_{Comp} set at $l = 1$, $l = 2$, $l = 3$ and $l = 4$, respectively. The dashed black line represents the evaluation of ε_ρ and ε_v for the purely compressible approach. The solid black line represents a second order slope.

reach eventually a plateau. This suggest that solving the low-Mach-number equations on additional levels of mesh refinement strongly reduced the error made on the convection of the entropy spot, but that the numerical errors made because of the poor resolution of the acoustic wave on the coarser mesh still remain in the solution at the finest level.

Furthermore, the same observations can be made from Figure 2.(b). Recall that only contributions from the vorticity mode should appear in the solution, solving the low-Mach-number equations on additional finer levels should strongly reduce ε_v. However, a significant error remains on ε_v when $l_{\mathrm{Comp}} = 1$ and 2, even at the finest level of refinement for the low-Mach-number equations. This suggests that numerical errors from the poor resolution of the acoustic wave appear in the low-Mach-number solution. For $l_{\mathrm{Comp}} = 3$, the acoustic wave is considered enough well resolved, so that numerical errors from the purely compressible equations become negligible and the contribution of additional low-Mach-number levels is significant to reduce the overall error made on the velocity. This is consistent with the observation made in Figure 2.(a) that the error in the density has reached a plateau for $l_{\mathrm{Comp}} > 3$.

This study exhibits the limitations of the hybrid method. Solving the low-Mach-number equations on additional level of mesh refinement only provides a better solution for phenomena that do not include contributions from the acoustics. This suggests that acoustic phenomena of interest must still be well enough resolved on the levels where the purely compressible equations are solved. This is obvious with the present test case. For example in Figure 2.(a), for $l_{\mathrm{Comp}} = 3$ and 4, the hybrid method provides an error ε_ρ that is similar to the error made with the purely compressible approach (dashed line).

However, the interest of the hybrid method developed in the present paper is highlighted in Figures 3 and 4. Figure 3 presents the comparison of the average time-step employed during simulations performed with the purely compressible approach (dashed line) and the hybrid method (symbols). For the hybrid method, similarly to Figures 2.(a) and 2.(b), the circle, diamond, square and cross symbols represent l_{Comp} set at $l = 1$, $l = 2$, $l = 3$ and $l = 4$, respectively. They obviously collapse in the same curve because the finest level of mesh refinement L determines the low-Mach-number time-step Δt_{LM}. On the other hand, Figure 4

presents the overall wall-clock computational time corresponding to the simulations performed in the present section. Together with the results presented in Figure 3 and Figures 2.(a) and 2.(b), two major general observations can be made:

- When l_{Comp} is too coarse, solving the low-Mach-number equations on additional levels of mesh refinement does not help to capture a good representation of the physics, or to provide a significant gain in the computational time.
- once the physics specifically related to generation of the acoustics is well enough resolved by selecting the proper level of discretization l_{Comp}, solving the low-Mach-number equations on a few additional levels provides a significant gain in both the computational and the numerical error of the solution. This is particularly true for the configuration $l_{\text{Comp}} = 4$ and $L = 5$: the hybrid method provides a discretization error in the density which is lower than the purely compressible approach, while at the same time exhibiting a computational cost about twice less expensive (see Figure 3).

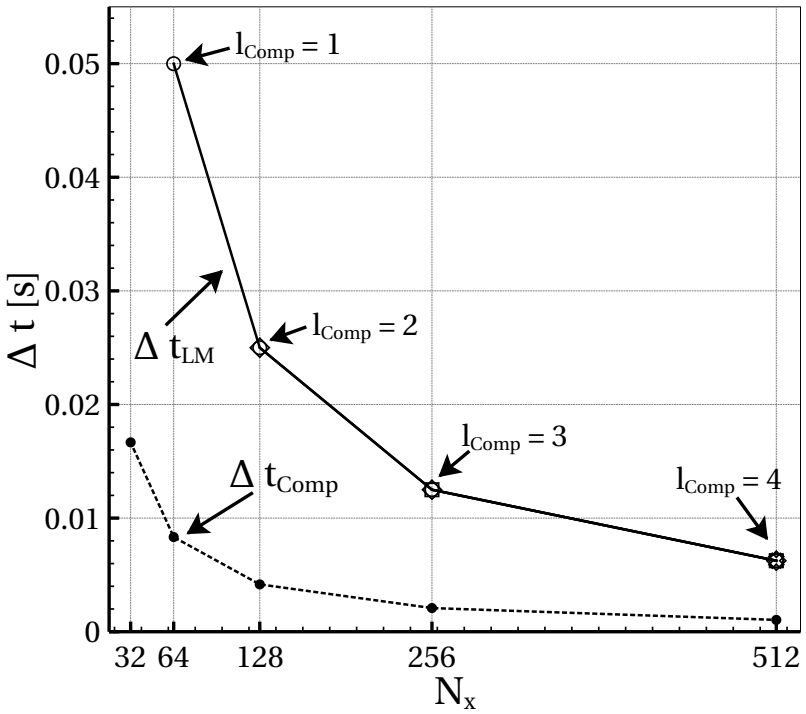

Figure 3. Average time-step employed during simulations performed with the purely compressible approach (dashed line) and the hybrid method (symbols), and for different maximum level L of mesh refinement for the low-Mach-number equations. For the hybrid method, circle, diamond, square and cross symbols represent l_{Comp} set at $l = 1$, $l = 2$, $l = 3$ and $l = 4$, respectively.

The present test case highlights the capacity of the hybrid method to retain acoustic phenomena within the context of a low-Mach-number solver. The major trend highlighted here is that acoustic phenomena must be well enough resolved where the fully compressible equations are solved. It is however emphasized that this test case is very canonical because the acoustics and the rest of the dynamic of the flow are, in the same time, well defined and decoupled from each other. For practical applications, the goal is to solve the low-Mach-number equations only in regions of the domain where the Mach number is small – hence the computational savings due to the larger low-Mach-number time step are greatest – and where the flow features have very fine structure that must be resolved. Such practical application will be investigated in a subsequent paper by the computation of the aeroacoustic sound generated by the vortex formation from a Kelvin-Helmholtz instability in low-Mach-number mixing layers.

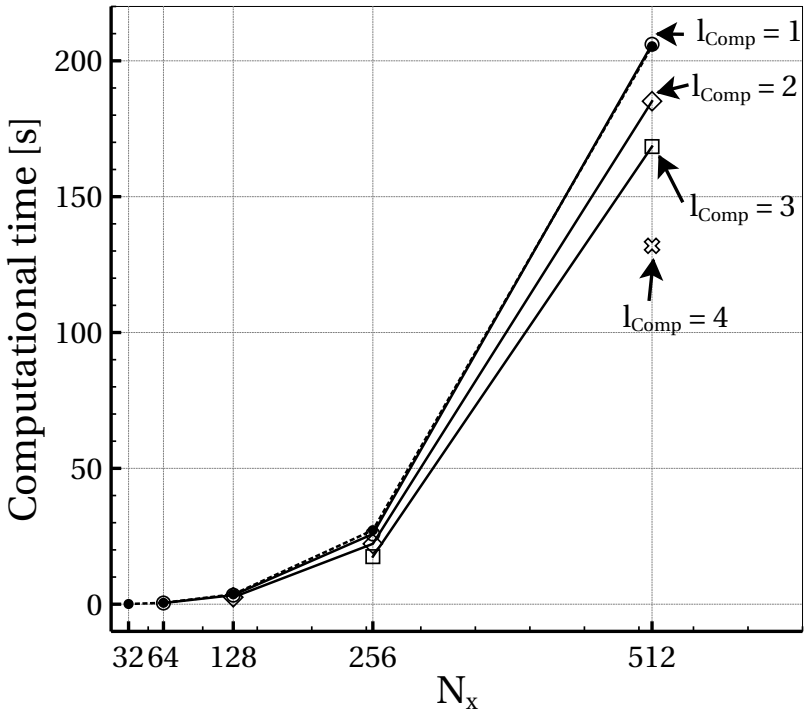

Figure 4. Wall-clock computational time spent to perform simulations with the purely compressible approach (dashed line) and the hybrid method (symbols), and for different maximum level L of mesh refinement for the low-Mach-number equations. For the hybrid method, circle, diamond, square and cross symbols represent l_{Comp} set at $l = 1$, $l = 2$, $l = 3$ and $l = 4$, respectively.

IV. Conclusions

A novel hybrid strategy has been presented in this paper to simulate flows in which the primary features of interest do not rely on high-frequency acoustic effects, but in which long-wavelength acoustics play a nontrivial role and present a computational challenge. Instead of integrating the whole computational domain with the purely compressible equations, which can be prohibitively expensive due to the CFL time step constraint, or with only the low-Mach-number equations, which would remove all acoustic wave propagation, an algorithm has been developed to couple the purely compressible and low-Mach-number equations. In this new approach, the fully compressible Euler equations are solved on the entire domain, eventually with local refinement, while their low Mach number counterparts are solved on specific sub-regions of the domain with higher spatial resolution. The coarser acoustic solution communicates inhomogeneous divergence constraints to the finer low-Mach-number grid, so that the low-Mach-number method retains the long-wavelength acoustics. This strategy fits naturally within the paradigm of block-structured adaptive mesh refinement (AMR) and the present algorithm is developed within the BoxLib framework that provides support for the development of parallel structured-grid AMR applications.

The performance of the hybrid algorithm has been demonstrated on a test case consisting on the combination of mixed modes composed of the propagation of a circular acoustic wave together with the convection of an entropy spot superimposed to a circular vortex. It has been shown that the acoustic phenomena must be well enough resolved and that solving the low-Mach-number equations on additional levels of mesh refinement helps to get a better solution on other flow phenomena not directly related to the acoustics.

The hybrid method presented in this paper is a first step in the development of a new kind of algorithm to solve problems that feature a large discrepancy in spatial and temporal scales within the same domain. This opens the way to efficient simulations of complex and multi-physics problems such as combustion instabilities

in industrial configurations.

Acknowledgments

The work here was supported by the U.S. Department of Energy, Office of Science, Office of Advanced Scientific Computing Research, Applied Mathematics program under contract number DE-AC02005CH11231. Part of the simulations were performed using resources of the National Energy Research Scientific Computing Center (NERSC), a DOE Office of Science User Facility supported by the Office of Science of the U.S. Department of Energy under Contract No. DE-AC02-05CH11231.

References

[1]Majda, A. and Sethian, J., "The Derivation and Numerical Solution of the Equations for Zero Mach Number Combustion," *Combust. Sci. Tech.* , Vol. 42, No. 3-4, 1985, pp. 185–205.

[2]McMurtry, P. A., Jou, W.-H., Riley, J., and Metcalfe, R. W., "Direct numerical simulations of a reacting mixing layer with chemical heat release," *AIAA Journal* , Vol. 24, No. 6, Jun 1986, pp. 962–970.

[3]Day, M. S. and Bell, J. B., "Numerical simulation of laminar reacting flows with complex chemistry," *Combust. Theory and Modelling* , Vol. 4, No. 4, 2000, pp. 535–556.

[4]Najm, H. N., Valorani, M., Goussis, D. A., and Prager, J., "Analysis of methane–air edge flame structure," *Combust. Theory and Modelling* , Vol. 14, No. 2, 2010, pp. 257–294.

[5]Knikker, R., "A comparative study of high-order variable-property segregated algorithms for unsteady low Mach number flows," *Int. J. Numer. Meth. Fluids* , Vol. 66, No. 4, 2011, pp. 403–427.

[6]Aspden, A., Day, M., and Bell, J., "Three-dimensional direct numerical simulation of turbulent lean premixed methane combustion with detailed kinetics," *Combust. Flame* , Vol. 166, 2016, pp. 266–283.

[7]Motheau, E. and Abraham, J., "A high-order numerical algorithm for DNS of low-Mach-number reactive flows with detailed chemistry and quasi-spectral accuracy," *J. Comput. Phys.* , Vol. 313, 2016, pp. 430–454.

[8]Wang, Z., Motheau, E., and Abraham, J., "Effects of equivalence ratio variations on turbulent flame speed in lean methane/air mixtures under lean-burn natural gas engine operating conditions," *Proc. Combust. Inst.* , Vol. 36, No. 3, 2017, pp. 3423–3430.

[9]Huang, Y. and Yang, V., "Dynamics and stability of lean-premixed swirl-stabilized combustion," *Prog. Energy Comb. Sci.* , Vol. 35, No. 4, 2009, pp. 293–364.

[10]Gicquel, L., Staffelbach, G., and Poinsot, T., "Large Eddy Simulations of gaseous flames in gas turbine combustion chambers," *Prog. Energy Comb. Sci.* , Vol. 38, No. 6, 2012, pp. 782–817.

[11]Lieuwen, T. C., *Unsteady combustor physics*, Cambridge University Press, 2012.

[12]Candel, S., Durox, D., Schuller, T., Darabiha, N., Hakim, L., and Schmitt, T., "Advances in combustion and propulsion applications," *European Journal of Mechanics - B/Fluids*, Vol. 40, 2013, pp. 87–106, Fascinating Fluid Mechanics: 100-Year Anniversary of the Institute of Aerodynamics, {RWTH} Aachen University.

[13]Motheau, E., Nicoud, F., and Poinsot, T., "Mixed acoustic-entropy combustion instabilities in gas turbines," *J. Fluid Mech.* , Vol. 749, 6 2014, pp. 542–576.

[14]Poinsot, T., "Prediction and control of combustion instabilities in real engines," *Proc. Combust. Inst.* , Vol. 36, No. 1, 2017, pp. 1–28.

[15]Roller, S. and Munz, C.-D., "A low Mach number scheme based on multi-scale asymptotics," *Comput. Vis Sci.* , Vol. 3, No. 1, 2000, pp. 85–91.

[16]Munz, C.-D., Roller, S., Klein, R., and Geratz, K., "The extension of incompressible flow solvers to the weakly compressible regime," *Comput. Fluids* , Vol. 32, No. 2, 2003, pp. 173–196.

[17]Park, J. H. and Munz, C.-D., "Multiple pressure variables methods for fluid flow at all Mach numbers," *Int. J. Numer. Meth. Fluids* , Vol. 49, No. 8, 2005, pp. 905–931.

[18]Munz, C.-D., Dumbser, M., and Roller, S., "Linearized acoustic perturbation equations for low Mach number flow with variable density and temperature," *J. Comput. Phys.* , Vol. 224, No. 1, 2007, pp. 352–364, Special Issue Dedicated to Professor Piet Wesseling on the occasion of his retirement from Delft University of Technology.

[19]Zhang, W., Almgren, A., Day, M., Nguyen, T., Shalf, J., and Unat, D., "BoxLib with Tiling: An Adaptive Mesh Refinement Software Framework," *J. Sci. Comput.* , Vol. 38, No. 5, 2016, pp. S156–S172.

[20]Bell, J. B. et al., *BoxLib User's Guide.*, 2016, https://ccse.lbl.gov/BoxLib/.

[21]Almgren, A. S., Beckner, V. E., Bell, J. B., Day, M. S., Howell, L. H., Joggerst, C. C., Lijewski, M. J., Nonaka, A., Singer, M., and Zingale, M., "CASTRO: A New Compressible Astrophysical Solver. I. Hydrodynamics and Self-gravity," *Astrophys. J.* , Vol. 715, No. 2, 2010, pp. 1221.

[22]Nonaka, A., Almgren, A. S., Bell, J. B., Lijewski, M. J., Malone, C. M., and Zingale, M., "MAESTRO: An Adaptive Low Mach Number Hydrodynamics Algorithm for Stellar Flows," *Astrophys. J., Suppl. Ser.*, Vol. 188, No. 2, 2010, pp. 358.

[23]Tam, C. K. M. and Webb, J. C., "Dispersion-Relation-Preserving Finite Difference Schemes for Computational Acoustics," *J. Comput. Phys.* , Vol. 107, 1993, pp. 262–281.